

LETTER TO THE EDITOR

ALMA CO and VLT/SINFONI H₂ observations of the Antennae overlap region: mass and energy dissipation [★]

C. N. Herrera^{1**}, F. Boulanger¹, N. P. H. Nesvadba¹, and E. Falgarone²

¹ Institut d'Astrophysique Spatiale, UMR 8617 CNRS, Université Paris-Sud 11, 91405 Cedex Orsay, France

² LERMA, UMR 8112 CNRS, Ecole Normale Supérieure and observatoire de Paris, Paris, France

Preprint online version: August 17, 2018

ABSTRACT

We present an analysis of super-giant molecular complexes (SGMCs) in the overlap region of the Antennae galaxy merger, based on ALMA CO(3–2) interferometry and VLT/SINFONI imaging spectroscopy of H₂ 1–0 S(1) at angular resolutions of 0.9'' and 0.7'', respectively. All but one SGMC have multiple velocity components offset from each other by up to 150 km s⁻¹. H₂ line emission is found in all SGMCs and the kinematics of H₂ and CO are well matched. H₂/CO line ratios vary by up to a factor of 10 among SGMCs and different velocity components of the same SGMCs. We also identify the CO counterpart of a bright, compact source of near-IR H₂ line emission, which shows no Br_γ, and was first identified with SINFONI. This source has the highest H₂/CO line ratio, and coincides with the steepest CO velocity gradient of the entire overlap region. With a size of 50 pc and a virial mass of a few 10⁷ M_⊙, it is perhaps a pre-cluster cloud that has not yet formed significant numbers of massive stars. We present observational evidence that the H₂ emission is powered by shocks, and demonstrate how the H₂ 1–0 S(1) and the CO(3–2) lines can be used as tracers of energy dissipation and gas mass, respectively. The variations in the H₂/CO line ratio may indicate that the SGMCs are dissipating their turbulent kinetic energy at different rates. The compact source could represent a short (~ 1 Myr) evolutionary stage in the early formation of super-star clusters.

Key words. Galaxies: individual: Antennae – Galaxies:ISM – Radio lines: ISM – Infrared: ISM – Turbulence

1. Introduction

Major gas-rich mergers are important sites of star formation and galaxy evolution in the Universe. The Antennae galaxy merger (NGC4038/4039) is an ideal target for studying in detail how galaxy interactions affect the interstellar medium and star formation. Most stars in the Antennae form in super-star clusters (SSCs) with stellar masses up to a few 10⁶ M_⊙ (Whitmore et al. 2010) located where the two galaxies permeate each other, the 'overlap region'. Super-giant molecular complexes (SGMCs) with masses of several 10⁸ M_⊙ and sizes of ~500 pc have been identified in CO(1–0) in the overlap region with the OVRO interferometer (Wilson et al. 2000). Ueda et al. (2012) have recently reported higher resolution (~ 100 pc), CO(3–2) observations of the Antennae obtained with the SMA.

The formation of SSCs involves a complex interplay of merger-driven gas dynamics, turbulence fed by the galaxy interaction, and dissipation of the kinetic energy of the gas. Hydrodynamic simulations suggest that massive complexes of cold gas, akin to SGMCs, form where gas flows trigger compression, cooling and gravitational fragmentation (Teyssier et al. 2010). Within SGMCs, a hierarchy of structures must form including clouds that are sufficiently massive to form SSCs (Weidner et al. 2010).

Recent VLT/SINFONI imaging spectroscopy of the peak of pure-rotational H₂ emission in the overlap region previously observed with Spitzer (Herrera et al. 2011, H11 hereafter) revealed

bright diffuse H₂ line emission associated with an SGMC and a compact (~0.6'', ~50 pc) source. H11 proposed that the compact source may be a massive cloud on its way to form a SSC within the next few Myr. The H₂ lines are powered by shocks and trace energy that is being dissipated and radiated away as the cloud complex, and a pre-cluster cloud (PCC) within, grow through gas accretion.

Herrera et al. (2011) had sub-arcsecond resolution SINFONI data of shocked gas, but lacked CO observations at similar resolution, which are required to probe the bulk of the gas on the relevant scales of ≤100 pc. In this letter, we take advantage of the recently released ALMA science verification observations of CO(3–2) in band 7 (~345 GHz) at ~1'' angular resolution to compare the morphology and kinematics of CO(3–2) and H₂ line emission in the Antennae overlap region. We show that together the ALMA and VLT observations provide the complementary (mass and energetics) data needed to characterize the dynamical state of SGMCs and to search for pre-cluster clouds.

2. Comparison of ALMA and SINFONI observations

Our analysis relies on two data sets. First, CO(3–2) line emission was obtained during ALMA science verification. These data are part of a mosaic of the Antennae obtained in 10 hr of observing time in band 7 (345 GHz) between May and June 2011, with 10 to 13 antennae and baselines from 25 to 200 m. This gives an angular resolution of 0''.6×1''.1 (66 pc×115 pc, at a distance of 22 Mpc) and covers the entire overlap region. The data have an intrinsic spectral resolution of 0.85 km s⁻¹ and were binned into channels of 10 km s⁻¹. We used the reduced data

[★] Based on ALMA Science Verification data and observations with the VLT/SINFONI, Program IDs 383.B-0789 and 386.B-0942.

^{**} supported by a CNRS-CONICYT grant.

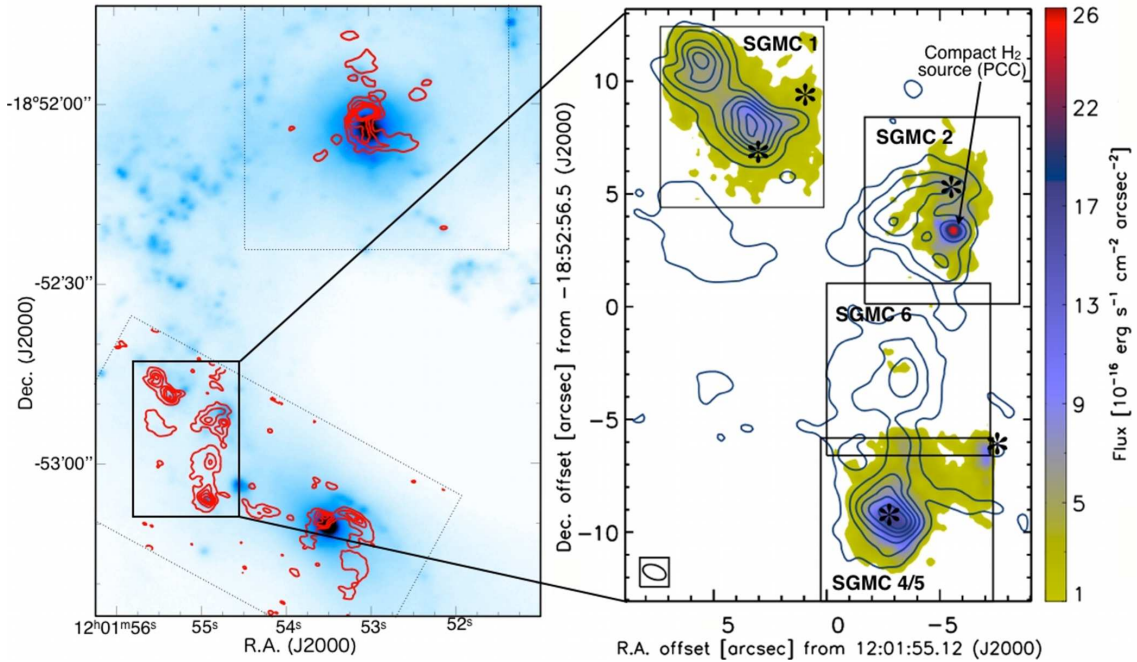


Fig. 1. *Left.* ALMA CO morphology shown on top of our CFHT K-band continuum image (H11). Dotted boxes mark the two ALMA mosaics, the solid box marks the overlap region. *Right.* H₂ 1–0 S(1) morphology as seen with SINFONI. Boxes mark individual SINFONI fields-of-view, contours show CO(3–2) from 2 to 42 Jy km s^{−1} beam^{−1} in steps of 8 Jy km s^{−1} beam^{−1}. The inset at the bottom left of the right panel shows the ALMA beam. We also mark massive and young SSCs (asterisks), and the compact H₂ source PCC discussed in § 3.

cubes publicly available on the ALMA website¹, which we corrected for the primary beam attenuation. Low spatial frequencies were filtered out because of missing short spacings that cause a loss of extended structures $>4''$ and negative sidelobes adjacent to bright emission. To measure fluxes we used a clipped cube where all pixel values $<2\sigma$ (6 mJy beam^{-1}) were set to zero. To quantify the missing flux, we constructed spectra at the center of the overlap region with the angular resolution of the single-dish JCMT and HHT CO(3–2) observations of Zhu et al. (2003) and Schulz et al. (2007), respectively. We found about half the total flux of the single-dish data. The total flux of the SGMCs in the overlap region agrees with the SMA observations (Ueda et al. 2012). Second, we used VLT/SINFONI imaging spectroscopy of ro-vibrational H₂ lines in the near-infrared *K*-band at $R=3000$ in four regions each $8'' \times 8''$ in size (Fig. 1). They were observed in February 2011 with on-source integration times of 40 minutes per pointing. Our previous observations of SGMC 2 have been discussed by H11. We obtained and reduced the data of the three additional fields in a similar way.

Fig. 1 shows the spatial distribution of the H₂ and CO emission in the Antennae overlap region at a spatial resolution of $\leq 1''$ (100 pc). The right panel displays the color image of the H₂ 1–0 S(1) emission with CO(3–2) contours for comparison. Intensity maps were obtained from the SINFONI and ALMA data cubes by fitting Gaussian profiles to the spectra in each spatial pixel, using one component for SINFONI and up to three components for the higher spectral resolution ALMA data. In Fig. 2 we compare the velocity fields of these two lines. For the CO velocities we computed the first moment map, and for H₂ we constructed the velocity map from Gaussian fits.

The ALMA channel maps are very similar to the SMA observations in Ueda et al. (2012). We identified all SGMCs discovered by Wilson et al. (2000) except for SGMC 3, which is

not covered by ALMA. The new data show two velocity components in SGMC 1 and 2. We also decomposed SGMC 4/5 into two smaller complexes at positions $(-3, -9.5)$ and $(-3, -3.5)$ in Fig. 1, each of which has two velocity components. We kept the name SGMC4/5 for the first complex, and labeled the northern extension SGMC 6. CO and H₂ spectra of each SGMC are displayed in Fig. 2. The CO spectra were integrated over each box in Fig. 1 using the clipped cube.

Table 1 lists the CO line properties of each SGMC and each velocity component, named a and b. Fluxes, velocities and line widths of all components are measured from Gaussian fits to the spectra in Fig. 2. Error bars include only fit uncertainties, not the systematic errors owing to the missing short spacings. We estimated the $R_{3-2/1-0} = I_{\text{CO}(3-2)} / I_{\text{CO}(1-0)}$ ratios of the SGMCs by comparing the ALMA and OVRO data, after smoothing to a common resolution. I_{CO} is the integrated intensity in K km s^{−1}. This ratio varies from source to source between 0.3–0.8, with a mean value of 0.5, consistent with what Schulz et al. (2007) found from single-dish data for the entire overlap region, as well as the peak line ratios measured with the SMA for each individual SGMC (Ueda et al. 2012).

We estimated gas masses from the CO fluxes, where the X_{CO} factor is the main source of uncertainty. To be consistent with previous studies, we used the same X_{CO} factor for CO(1–0) as Wilson et al. (2000), $X_{\text{CO}} = 3 \times 10^{20} \text{ H}_2 \text{ cm}^{-2} (\text{K km s}^{-1})^{-1}$, and adopted the scaling $R_{3-2/1-0} = 0.59$ of Schulz et al. (2007). Our mass estimates (Tab. 1) are comparable to those of Wilson et al. (2000). Similar to H11, our data show that most of the H₂ emission away from SSCs is powered by shocks, not UV heating in PDRs. The observed H₂ 2–1/1–0 S(1) ratios, 0.1–0.2 (Tab. 1) can be accounted for by PDR models, but only for high UV fields ($\chi > 10^4$, in units of the mean value in the solar neighborhood) and high densities ($n_{\text{H}} > 10^5 \text{ cm}^{-3}$, Le Petit et al. 2006). These conditions exist near massive stars embedded in molecular clouds, but the extended H₂ emission is generally not observed

¹ <http://almascience.eso.org/alma-data/science-verification>

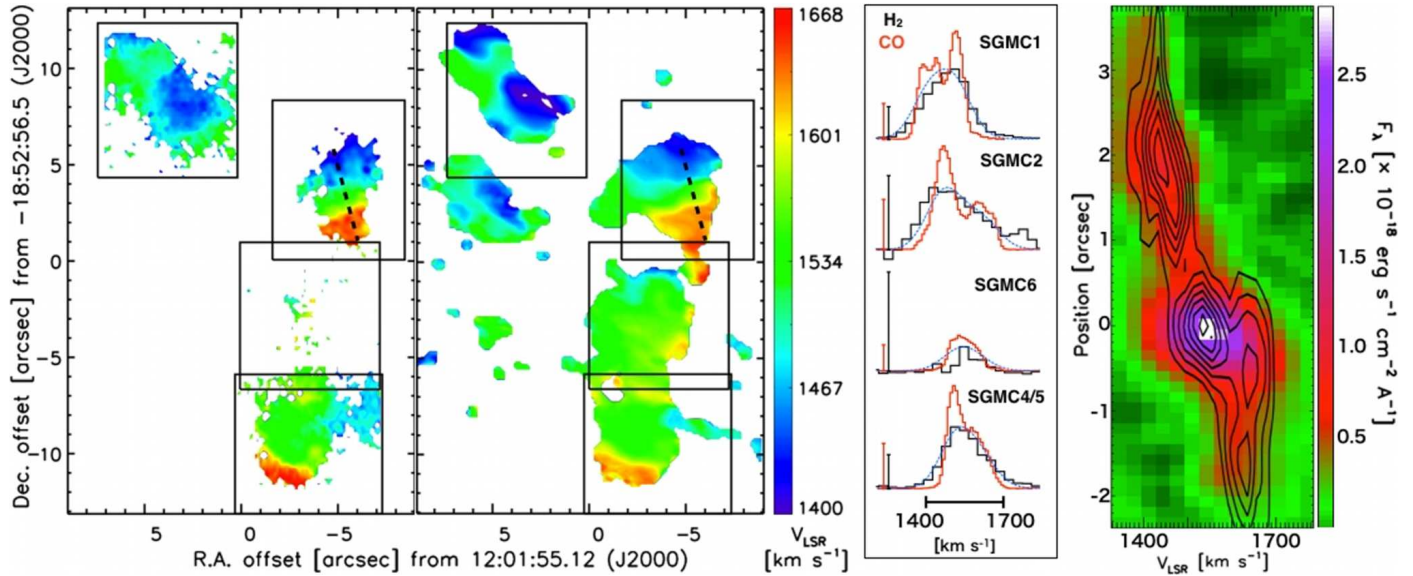


Fig. 2. *Left panel:* Velocity map of H₂ 1–0 S(1) (left) and first-moment map of CO(3–2) (right). Dotted lines mark the position-velocity cut shown in the right panel. *Mid panel:* Integrated line profiles of CO(3–2) (red) and H₂ 1–0 S(1) (black) for each SGMC. Blue spectra show the CO(3–2) lines convolved to the spectral resolution of SINFONI. Black bars correspond to 5×10^{-16} erg s⁻¹ cm⁻² Å⁻¹ for H₂ 1–0 S(1) and red bars to 1.5 Jy for CO(3–2), for all SGMCs. Offsets between the black and blue spectra indicate variations in the CO-to-H₂ ratio between velocity components. *Right panel:* H₂ 1–0 S(1) position-velocity diagram of SGMC 2 (H11), with CO(3–2) emission shown as contours in steps of 0.02 Jy beam⁻¹ starting at 0.03 Jy beam⁻¹.

to peak near the brightest SSCs. The notable exception is the embedded cluster in SGMC4/5, which, however, has a higher line ratio (Gilbert et al. 2000). In addition, the [CII]157μm/[OI]63μm line ratio indicates that the mean radiation field in the overlap region is $\chi \sim 10^3$ (Schulz et al. 2007), an order of magnitude smaller than that required to account for the H₂ 2–1/1–0 S(1) ratios. The other luminous SSCs have already dispersed most of their gas and dust. Thus, the brightest UV-heated gas would come from clouds away from the clusters. Outside the clusters the intensity of the radiation field is not very high. For a $5 \times 10^6 M_{\odot}$ SSC, the UV field is $\chi > 10^4$ only out to a distance of < 100 pc from the cluster and less if we include extinction.

Our analysis has three main results. (1) All SGMCs have H₂ 1–0 S(1) line emission and the H₂ 1–0 S(1) kinematics match those of CO(3–2) well. Zhu et al. (2003) and Schulz et al. (2007) found that the CO is emitted from gas at temperatures with $T \sim 30$ –150 K. The excitation temperature of the warmer H₂ gas emitting in the near-IR is ~ 1000 –2000 K (H11). The similarity of the gas kinematics of CO and H₂ indicates that warm and cold gas are closely associated. (2) Figs. 1 and 2 show large variations in the H₂/CO ratio between SGMCs and between individual velocity components in the same SGMC (Tab. 1). Extinction is an unlikely cause, because the near- and mid-IR H₂ pure-rotational emission-line regions have similar morphologies (at least at the 5'' scales resolved by Spitzer-IRS; see Fig. 4 in Brandl et al. 2009, and the discussion in H11). In H11, we related the H₂ emission to the dissipation of kinetic energy. With this interpretation, the H₂/CO ratio traces differences in the energy dissipation rate per unit mass, which must be related to the dynamical evolution of the gas. (3) All clouds have two spatially separated velocity components as seen in the channel maps of SGMC 2 in Fig. 3. In the other clouds, the spatial offsets between velocity components are less obvious, possibly because of projection effects. The velocity difference between components within an individual SGMC is up to 150 km s⁻¹ (Fig. 2). Given the size and mass of the SGMCs, this is too large to be accounted

for by the gas self-gravity. The gas kinematics is most likely driven by the galaxy interaction. Single-dish observations found similar velocity gradients in the extended emission around the SGMCs, which further supports this idea. The two components in SGMC 2 are spatially separated and resolved by ALMA. We estimated their sizes and found their virial masses to be comparable to the molecular masses derived from the CO fluxes.

3. The compact H₂ source

The ALMA maps also give new insight into the nature of the bright, compact H₂ emitter associated with SGMC 2, PCC, recently discovered by H11. PCC is the brightest H₂ line emitter in the overlap region. It is not detected in the lower-resolution CO(1–0) data, but is an emission peak in the SMA and ALMA maps (Fig. 1). Isolating the PCC CO counterpart from the surrounding extended emission is difficult with an algorithm like CLUMPFIND because of the large velocity gradient across PCC (see right panel in Fig. 2). This may explain why the source is not specifically listed in Table B.1 of Ueda et al. (2012). There is no other CO peak in the SGMCs with an obvious counterpart in the near-IR, except for the embedded SSC in SGMC 4/5.

Fig. 3 shows a comparison of the CO and CRIFES high-resolution (6 km s⁻¹) H₂ 1–0 S(1) spectra of PCC (H11). The CO spectrum is the peak emission at the position of the PCC corrected for the surrounding emission, measured over an annulus outside the source, to isolate the CO velocity component associated with the PCC. CO(3–2) and H₂ 1–0 S(1) spectra are remarkably similar. Table 1 lists the parameters of our Gaussian fit. The H₂-luminous PCC has a velocity dispersion (40 km s⁻¹) significantly higher than those of GMCs with the same sizes in the Milky Way (5 km s⁻¹; Falgarone et al. 2009; Heyer et al. 2009).

Using the velocity dispersion of CO(3–2), we obtain a virial mass of $M_{\text{vir}} = 5R\sigma^2/G = 4.6 \times 10^7 \times (\sigma_v/40 \text{ km s}^{-1})^2 M_{\odot}$. Since ALMA does not spatially resolve the PCC, we instead used the 50 pc size measured with SINFONI. The exceptionally

Table 1. CO(3–2) properties of the SGMCs (top) and PCC (bottom). We include the integrated H₂ 1–0 S(1) fluxes, and the H₂ 1–0/2–1 S(1) and H₂/CO flux ratios. For PCC, the line parameters are measured with a single-component Gaussian fit.

Source	Velocity component	V_{LSR} km s ⁻¹	Δv km s ⁻¹	S_{CO} Jy km s ⁻¹	M_{mol} M_{\odot}	$F_{\text{H}_2 \text{ 1-0 S(1)}}$ erg s ⁻¹ cm ⁻²	$\frac{F_{\text{H}_2 \text{ 2-1 S(1)}}}{F_{\text{H}_2 \text{ 1-0 S(1)}}$	$\frac{F_{\text{H}_2 \text{ 1-0 S(1)}}}{F_{\text{CO(3-2)}}$
SGMC 1	a	1417±2	105±6	380±24	$5.6 \pm 0.3 \times 10^8$	1.6×10^{-14}	0.2	2.1
	b	1521±1	63±3	289±16	$4.2 \pm 0.2 \times 10^8$			
SGMC 2	a	1469±1	90±2	289±8	$4.2 \pm 0.1 \times 10^8$	8.3×10^{-15}	0.2	1.6
	b	1613±2	114±5	176±10	$2.6 \pm 0.1 \times 10^8$			
SGMC 4/5	a	1505±1	58±2	171±9	$2.5 \pm 0.1 \times 10^8$	1.3×10^{-14}	0.3	2.6
	b	1586±3	126±6	256±12	$3.7 \pm 0.2 \times 10^8$			
SGMC 6	a	1506±2	50±8	48±12	$0.7 \pm 0.2 \times 10^8$	6.7×10^{-16}	<0.5 ^a	0.2
	b	1561±5	113±6	216±15	$3.2 \pm 0.2 \times 10^8$			
H ₂ source (PCC)	–	1534±2	93±4	7.6 ±0.4	$1.0 \pm 0.1 \times 10^7$	7.6×10^{-16}	0.1	8.7

^a H₂ 2–1 S(1) flux corresponds to an upper limit estimated from the noise.

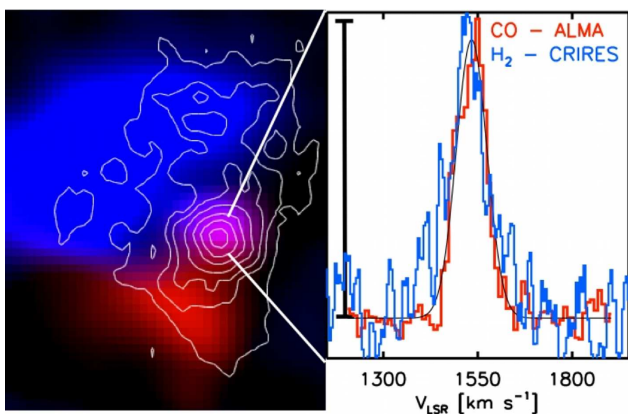


Fig. 3. (left) CO(3–2) emission from SGMC 2, where emission between 1350–1540 km s⁻¹ and between 1540–1750 km s⁻¹ are shown in blue and red, respectively. Contours show the H₂ 1–0 S(1) morphology. (right) CO(3–2) (red) and CRIRES H₂ (blue) spectrum of PCC. The H₂ spectrum is smoothed to 18 km s⁻¹ resolution. The bar corresponds to 77 mJy beam⁻¹ for CO(3–2) and 4.4×10^{-17} erg s⁻¹ cm⁻¹ Å⁻¹ for H₂ 1–0 S(1).

high H₂ 1–0 S(1)-to-Bry line ratio (>15, H11) provides unambiguous evidence that the H₂ emission of the PCC is powered by shocks (Puxley et al. 1990). The H₂/CO ratio, i.e. the energy dissipation rate per unit mass, is also exceptionally high, a factor 5 higher than that of the SGMC 2 complex overall.

PCC appears to be located at the interface between blue and redshifted gas (Fig. 3) where CO shows a steep velocity gradient (~ 1 km s⁻¹ pc⁻¹ in the position-velocity diagram in Fig. 2). The observed properties of PCC are consistent with a scenario where the formation of SSCs is triggered by interactions between two gas flows. In SGMC 2, depending on the full three-dimensional geometry, the flows could either be colliding or creating a large velocity shear, and most likely a combination of both. In either case, the interaction drives a turbulent energy cascade in which kinetic energy is being dissipated. This is where we would expect the highest energy dissipation rate.

The bolometric luminosity of the PCC is $\sim 10^7 L_{\odot}$. Observations of, e.g., NGC 1333 (Maret et al. 2009) show that the bolometric luminosity of protostellar outflows is on the order of $10^5 L_{\odot} \times \dot{M}_{\text{wind}}$, where \dot{M}_{wind} is the stellar mass loss rate in $M_{\odot} \text{ yr}^{-1}$. The small embedded stellar mass of $M_{*} = 4 \times 10^4 M_{\odot}$ (H11) makes protostellar winds an implausible energy source.

The cloud luminosity may be accounted for by the dissipation of the cloud kinetic energy for a cloud mass of a few $10^7 M_{\odot}$ – a value comparable to the virial mass $5 \times 10^7 M_{\odot}$ – and a dissipation timescale of 1 Myr. This is comparable to the cloud crossing time, and also the dynamical time scale associated with the velocity gradient of 1 km s⁻¹ pc⁻¹ at the position of the cloud. The similarity of both timescales indicates that the cloud may still be forming by accreting gas, and therefore that a significant part of the cloud luminosity may be powered by gas accretion. In any case, the time during which the PCC is a bright H₂ emitter is short, about 1 Myr.

This short timescale may explain why we do not find more bright compact sources in our new H₂ data. Whitmore et al. (2010) list five massive ($>10^5 M_{\odot}$), young (< 5 Myr) SSCs over the part of the overlap region covered with both ALMA and SINFONI (Fig. 1). This is consistent with finding only a single bright PCC with the SINFONI data if the H₂-luminous phase does not last longer than a few Myr.

Our analysis gives a foretaste of the power of combining mass and energy tracers to study the dynamical state of molecular gas in galaxy mergers and the early stages of the formation of SSCs. In the future, this approach can be extended with ALMA and VLT using additional tracers of energy dissipation and mass.

Acknowledgements. We wish to thank the staff at ALMA and the VLT for making these observations and are particularly grateful to the ALMA SV team for making the fully reduced and calibrated ALMA data available (ADS/JAO.ALMA#2011.0.00003.SV). We thank R. Kneissl for helping us in analyzing the ALMA SV maps, C. Wilson for providing us with her CO(1–0) OVRO data cube, and P. Guillard for his useful comments. We thank the referee for comments that improved our paper.

References

- Brandl, B. R., Snijders, L., den Brok, M., et al. 2009, *ApJ*, 699, 1982
 Falgarone, E., Pety, J., & Hily-Blant, P. 2009, *A&A*, 507, 355
 Gilbert, A. M., Graham, J. R., McLean, I. S., et al. 2000, *ApJ*, 533, L57
 Herrera, C. N., Boulanger, F., & Nesvadba, N. P. H. 2011, *A&A*, 534, A138
 Heyer, M., Krawczyk, C., Duval, J., & Jackson, J. M. 2009, *ApJ*, 699, 1092
 Le Petit, F., Nehmé, C., Le Bourlot, J., & Roueff, E. 2006, *ApJS*, 164, 506
 Maret, S., Bergin, E. A., Neufeld, D. A., et al. 2009, *ApJ*, 698, 1244
 Puxley, P. J., Hawarden, T. G., & Mountain, C. M. 1990, *ApJ*, 364, 77
 Schulz, A., Henkel, C., Muters, D., et al. 2007, *A&A*, 466, 467
 Teyssier, R., Chapon, D., & Bournaud, F. 2010, *ApJ*, 720, L149
 Ueda, J., Iono, D., Petitpas, G., et al. 2012, *ApJ*, 745, 65
 Weidner, C., Bonnell, I. A., & Zinnecker, H. 2010, *ApJ*, 724, 1503
 Whitmore, B. C., Chandar, R., Schweizer, F., et al. 2010, *AJ*, 140, 75
 Wilson, C., Scoville, N., Madden, S., & Charmandaris, V. 2000, *ApJ*, 542, 120
 Zhu, M., Seaquist, E. R., & Kuno, N. 2003, *ApJ*, 588, 243